

Artificial Neural Networks generated by Low Discrepancy Sequences

Alexander Keller and Matthijs Van keirsbilck

Abstract Artificial neural networks can be represented by paths. Generated as random walks on a dense network graph, we find that the resulting sparse networks allow for deterministic initialization and even weights with fixed sign. Such networks can be trained sparse from scratch, avoiding the expensive procedure of training a dense network and compressing it afterwards. Although sparse, weights are accessed as contiguous blocks of memory. In addition, enumerating the paths using deterministic low discrepancy sequences, for example the Sobol’ sequence, amounts to connecting the layers of neural units by progressive permutations, which naturally avoids bank conflicts in parallel computer hardware. We demonstrate that the artificial neural networks generated by low discrepancy sequences can achieve an accuracy within reach of their dense counterparts at a much lower computational complexity.

1 Introduction

The average human brain has about 10^{11} nerve cells, where each of them may be connected to up to 10^4 others. Yet, the complexity of artificial neural networks quite often is determined by fully connected sets of neurons. We therefore investigate algorithms for artificial neural networks that are linear in the number of neurons and explore their massively parallel implementation in hardware.

In order to reduce complexity, we motivate the principle of representing an artificial neural networks as paths instead of matrices in Sec. 2. Rather than creating such sparse networks by importance sampling paths from a trained dense network, training may be much more efficient when considering artificial neural networks that are sparse from scratch as discussed in Sec. 3. Enumerating the paths of an artificial neural network using a deterministic low discrepancy sequence and exploiting its structural properties, leads to an efficient hardware implementation, whose advan-

Alexander Keller · Matthijs Van keirsbilck
NVIDIA e-mail: akeller@nvidia.com, e-mail: matthijsv@nvidia.com

tages are detailed in Sec. 4. Initial numerical evidence to support the approach is reported in Sec. 5 before drawing the conclusions. A noteworthy result is that quasi-Monte Carlo methods enable a completely deterministic approach to artificial neural networks.

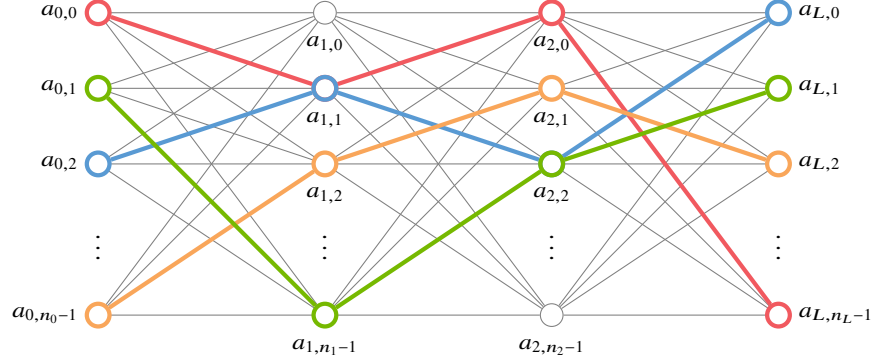


Fig. 1 Representing the graph of an artificial neural network by paths (colored) instead of fully connected layers (gray) allows for algorithms linear in the number of vertices in time and space.

2 Representing Artificial Neural Networks by Paths

In order to provide an intuition why representing artificial neural networks as paths may lower their computational complexity, we review their basic principles.

As depicted in Fig. 1, the computational graph of a basic artificial neural network may be organized in $L \in \mathbb{N}$ layers, each comprising of $n_l \in \mathbb{N}$ neural units, where $0 \leq l \leq L$. Given an input vector a_0 , the output vector a_L is computed layer by layer, where each vertex determines the activations

$$a_{l,i} := \max \left\{ 0, \sum_{j=0}^{n_{l-1}-1} w_{l,j,i} \cdot a_{l-1,j} \right\}. \quad (1)$$

For the purpose of the manuscript, it is sufficient to consider the non-linearity $\max\{0, x\}$ as an activation function, yielding the so-called rectified linear units (ReLU). The vertices of the graph are connected by edges with their associated weights $w_{l,j,i} \in \mathbb{R}$. In summary, each neural unit computes a weighted average of the activations in the previous layer. If the average is non-positive, it is clipped to zero, which renders the neural unit inactive. Otherwise the neural unit is called active and passes on the positive average.

In order to learn the weights from training data, backpropagation [RHW88] has become the most popular algorithm: Given an input vector a_0 and a desired output vector d , the approximation error

$$\delta_L := a_L - d \quad (2)$$

is propagated back through the network by computing the weighted average of the error

$$\delta_{l-1,i} := \sum_{a_{l,j} > 0} \delta_{l,j} \cdot w_{l,j,i} \quad (3)$$

of all active neural units in a layer. If a neural unit is active, the weight

$$w'_{l,j,i} := w_{l,j,i} - \lambda \cdot \delta_{l,j} \cdot a_{l-1,i} \text{ if } a_{l,j} > 0 \quad (4)$$

of an edge connecting it to a previous neural unit is updated by the product of the learning rate $\lambda \in \mathbb{R}^+$, the error at the active neural unit, and the activation of the previous neural unit.

As formalized by equation 1 and shown in Fig. 1, all neural units of one layer are connected to all neural units of the next layer. Such “fully connected” layers are found in many modern artificial neural networks, for example at the end of classification networks or as so-called 1x1-convolutions, which are fully connected layers with weight sharing across inputs. Obviously, the computational complexity as well as the number of weights of a layer is determined by the product of the number of neural units in the current and previous layer.

In order to motivate an algorithm linear in time and space, we rewrite the activations a_l in equation 1, which are the non-linearity applied to the average, equivalently as averages

$$z_{l,j} := \sum_{i=0}^{n_{l-1}-1} w_{l,j,i} \cdot \max\{0, z_{l-1,i}\}$$

of the non-linearity. Considering an integral

$$z_l(y) := \int_0^1 w_l(x, y) \cdot \max\{0, z_{l-1}(x)\} dx$$

rather than a sum, reveals that layers in artificial neural networks relate to high-dimensional integro-approximation. Hence, in continuous form, an artificial neural network is a sequence of linear integral operators applied to non-linear functions.

From the domain of integral equations, especially the domain of computer graphics, we know how to deal with such sequences: Sampling path space, we trace light transport paths that connect the light sources and camera sensors to render synthetic images. It now is obvious that an artificial neural network may be represented by paths that connect inputs and outputs, too. Computation only along the paths (colored in Fig. 1) yields a complexity in space and time that is linear in the number of paths times the depth of the neural networks and hence may be linear in the number of neural units.

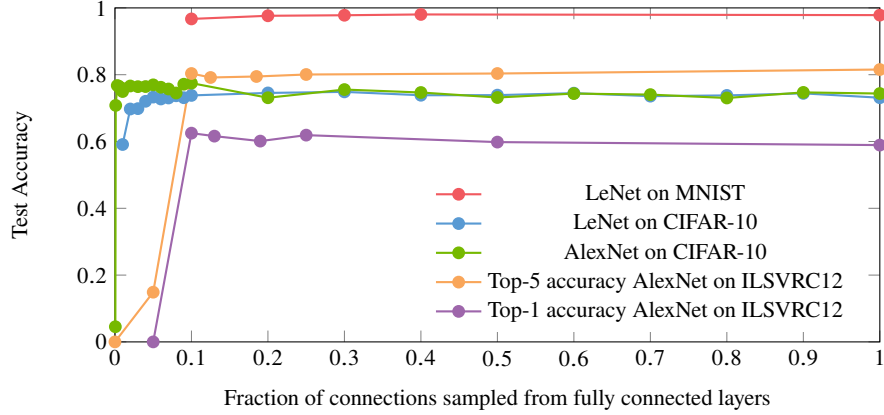


Fig. 2 Test accuracy of a selection of classic image recognition artificial neural networks. Using only about 10% (or even less) of the connections of the original trained networks does not result in a notable loss in test accuracy. The paths through the fully connected layers of the artificial neural networks have been sampled proportionally to the trained weights.

2.1 Quantization of Artificial Neural Networks by Sampling

In [MkK19] we derived an algorithm that quantizes a trained artificial neural network such that the resulting complexity may be linear. To create these paths given a trained neural network, we exploit an invariant of the rectified linear units (ReLU): In fact, scaling the activations by a positive factor $f \in \mathbb{R}^+$ and dividing the weighted average by the same factor leaves the result unchanged.

Choosing this factor as the one-norm of the weights of a neural unit, the factor can be propagated forward through the neural network, leaving the weights of each neural unit as a discrete probability density.

Given n weights, assuming $\sum_{k=0}^{n-1} |w_k| = \|w\|_1 = 1$ and defining a partition of the unit interval by $P_m := \sum_{k=1}^m |w_k|$, we have the following partitions:

$$0 = P_0 \quad \begin{array}{c} |w_1| \\ \hline \end{array} P_1 \quad \begin{array}{c} |w_2| \\ \hline \end{array} P_2 \quad \cdots \quad \begin{array}{c} |w_{n-1}| \\ \hline \end{array} P_{n-2} \quad P_{n-1} = 1$$

Now, it is straightforward to trace paths from the outputs back to the inputs by sampling proportional to the discrete densities. As they define partitions of one, a uniformly distributed sample x_i selects an activation by its associated probability. The graphs in Fig. 2 provide evidence that sampling only a fraction of the connections results in no notable degradation in the test accuracy. A similar approach can be used to quantize not just weights, but also activations and gradients to arbitrary precision. For more details and data, we refer to [MkK19] and [MkK20].

Above we used the L1-norm to generate probabilities from the weights. It is also possible to use more advanced importance estimation techniques. This can be used

both during training to precondition the model so it can be pruned to higher sparsity levels [MMT⁺19]. It’s also possible to use similar approaches to select subsets of neurons or weights to train, so a certain sparsity level is maintained throughout training for increased efficiency [DZ19] [JPR⁺20].

2.2 Sampling Paths in Convolutional Neural Networks (CNNs)

Convolutional neural networks [LBBH98] contain layers that compute features by convolutions. A convolutional neuron (also called filter or kernel) has a 3D tensor of weights with c_{in} input dimensions, width w_f , and height h_f . This means that each 2D slice of this kernel is convolved with the respective features of the c_{in} input dimensions. The convolution amounts to reusing the kernel across the width and height of the input dimensions, called ‘weight sharing’. Typically the support defined by the dimensions $w_f \times h_f$ is a rather small constant, for example 3×3 . As each of the neurons computes 1 output feature channel, the output dimension c_{out} equals the number of convolutional neurons. Typical sets of features computed by convolutional layers include edges of different orientations in an image, i.e. first and second derivatives.

Following the weight sharing paradigm, tracing a path through a convolutional layer amounts to selecting one of the c_{in} input dimensions. An activated path corresponds to selecting the weights of a $w_f \times h_f$ slice in the 3D tensor. Tracing paths that way through trained convolutional networks is closely related to ‘channel pruning’ [MMT⁺19]. This enables coarse sparsity on the filter level, which is more efficient on current hardware than fine-grained sparsity [CSZ17], i.e. selecting single weights.

Many recent CNN architectures such as MobileNet, DenseNet, or QuartzNet [KBG⁺20] use 1×1 -convolutions, where $w_f = h_f = 1$. This special case means that c_{in} input channels are mapped to c_{out} output channels, which amounts to a structure identical to a fully connected layer [HLVDMW17, CSZ17]. Sharing the weights across the elements of the activation tensor, paths can be traced in the same way as through fully connected layers.

For the sake of completeness, we mention that CNNs often contain MaxPooling layers that downsample the input tensor. As they share the same set of weights across a layer, too, paths through them are traced as described before.

3 Training an Artificial Neural Network Sparse from Scratch

Quantizing an artificial neural network by sampling paths still requires to train the full network. This complexity issue may be resolved by training an artificial neural network sparse from scratch as principled by the implementation provided in Fig. 3. We start by storing random paths as an array `index[][]` of indices. Therefore, we

Program Code

```

// initialization

int neurons = 0;

for (int l = 0; l < layers; ++l)
{
    for (int p = 0; p < paths; ++p)
        index[l][p] = neurons + (int) (drand48() * neuronsPerLayer[l]);

    neurons += neuronsPerLayer[l];
}

for (int l = 1; l < layers; ++l)
    for (int p = 0; p < paths; ++p)
        weight[l][p] = initialWeight; // deterministic instead of random

float *a = new float[neurons];
float *error = new float[neurons];

// train by backpropagation

...

// inference

for (int i = 0; i < neuronsPerLayer[0]; ++i)
    a[i] = inputs[i];

for (int i = neuronsPerLayer[0]; i < neurons; ++i)
    a[i] = 0.0f; // or bias[i], if bias terms are used

for (int l = 1; l < layers; ++l)
    for (int p = 0; p < paths; ++p)
        if (a[index[l - 1][p]] > 0.0f) // ReLU
            a[index[l][p]] += weight[l][p] * a[index[l - 1, p]];

```

Fig. 3 Implementation of an artificial neural network represented by paths using rectified linear units (ReLU) as activation functions. Given the numbers of `layers`, `paths`, and the array of `neuronsPerLayer`, the array `index` stores the indices of neural units along a path `p` created by randomly selecting a neural unit per layer. Before training by backpropagation, the `weight` of each edge is set to a constant `initialWeight`. For inference, the activations `a` of the first layer are set to the input data, while the remaining activations are set to zero. Enumerating all activations for all subsequent layers and for all paths, each activation along an edge is updated, if its previous activation along the path is active, i.e. larger than zero, which amounts to the rectified linear unit (ReLU) activation function.

enumerate all layers and paths. In layer l of path p , the index of a neural unit is just randomly selected among the neuron units of that respective layer.

The evaluation - also called inference - of an artificial neural network represented by paths first copies all inputs to an array of activations and then initializes all other activations to zero. The actual computation then loops over all layers and paths, where an activation is updated only if the previous vertex along the path p is positive, meaning active. This is an implicit implementation of the rectified linear neural unit (ReLU) introduced in equation 1.

In the same manner, restricting training by backpropagation [RHW88] as defined by equations 2, 3, and 4 to the representation by paths is straightforward. In analogy to Sec. 2.2, convolutional layers can be represented by paths and be trained sparse from scratch, too, resembling methods to create predefined sparse kernels [KPA⁺19, KNP⁺20].

It is obvious that the complexity of inference and training is linear in the number of paths times the depth of the neural network. Also note, that although sparse, all weights are accessed in linear order, which is the most efficient memory access pattern on modern computer hardware.

3.1 Constant Initialization

For a fully connected neural network, all neurons in a layer have the same connectivity, i.e. each neuron is connected to the same neurons in the previous and following layer. If all weights were initialized uniformly, all neurons would receive the same updates, and the network would learn nothing during training. The usual way to prevent this is to initialize the weights by sampling randomly from some distribution. There has been a lot of work done on finding good initializations, depending on the used activation function, size of weight tensor, and other factors [GBB11, HZRS15, dS16].

However with sparse networks, each neuron has a different connectivity pattern. Instead of introducing randomness by sampling random weights, the non-uniform connectivity pattern ensures that not every neuron learns the same thing. This allows one to get rid of the random initialization, as shown in the code in Fig. 3, where the weights along the edges of the paths are initialized with a constant.

The value of the constant itself is still important as it controls the operator norm of the affine transformation that each neuron performs. Following the analysis of [HZRS15], and considering that our networks use the ReLU activation function, we use $w_{\text{init}} = \frac{6}{\sqrt{\text{fan_in} + \text{fan_out}}}$, where `fan_in` is the number of inputs to a neural unit and `fan_out` the number of its connections to the next layer. Biases are initialized with 0, and scale and shift parameters of batch normalization layers are initialized with 1 and 0, respectively.

We may conclude that the classic random weight initialization required to make fully connected layers learn is replaced by the fact that in a artificial neural network sparse from scratch neural units don't share the same set of connections.

3.2 Non-negative Weights

Weights may change sign during training. Yet, it has been observed that a graph of an artificial neural network including static signs of the weights may be separated from training the magnitudes of the weights [FC19, ZLLY19]. However, finding this graph and its associated static signs requires pruning a trained, fully connected, and randomly initialized artificial neural network.

When working with optical implementations of artificial neural networks, only non-negative weights may be used, because either there is light or not [FPPP85]. The lack of negative weights is accounted for by amplifying differences of weighted sums similar to how operational amplifiers work. A modern example are ternary quantized artificial neural networks [ZHMD16], where a first binary matrix accounts for all non-negative weights of a layer, and a second binary matrix produces the sums to be subtracted. Still, finding the ternary representation requires pruning a fully connected network and retraining.

Representing artificial neural networks by paths, we propose to attach one fixed sign to each path. As paths are generated by random walks, selecting the weights of the even paths to be non-negative and the weights of the odd paths to be non-positive perfectly balances the number of positive and negative weights. Alternatively, any ratio of positive and negative weights may be realized by for example determining the sign of a path by comparing its index to the desired number of positive paths (even per layer). This architecture can be thought of as an inhibiting network superimposed on a supporting network. Such a network may be trained by, for example, backpropagation with the only restriction that weights cannot become negative.

3.3 Normalization

Being able to use a constant value for weight initialization allows one to fulfill normalization constraints. For example, knowing the number of edges incident to a neural unit, it is straightforward to determine the initial weight such that any selected p -norm of a set of weights will be one. Uniformly scaling the initial weights allows one to control the operator norm of the artificial neural network represented by paths [MkK19].

4 Low Discrepancy Sequences to enumerate Network Graphs

Low discrepancy sequences [Nie92, DP10] may be considered the deterministic counterpart of pseudo-random number generators. Abandoning the simulation of independence, they generate points in the unit hypercube much more uniformly distributed than random numbers ever can be. Improving convergence speed, they

have become the industry standard for generating light transport paths in computer graphics [Kel13, HBO⁺19].

Reviewing classic concepts of parallel computation (see Sec. 4.1), taking advantage of the properties of low discrepancy sequences (see Sec. 4.2) results in an algorithm to enumerate the graph of an artificial neural network (see Sec. 4.3) that is perfectly suits an implementation in massively parallel hardware (see Sec. 4.4).

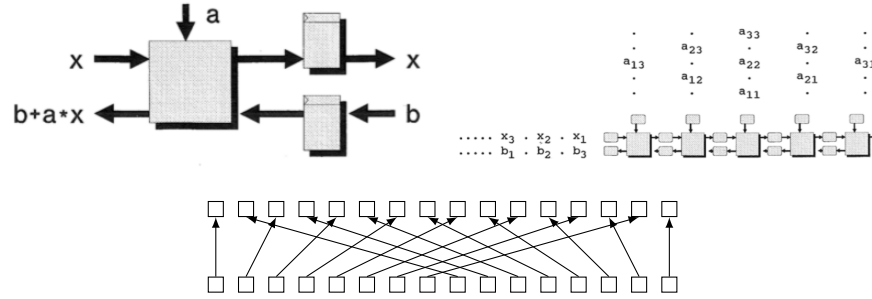


Fig. 4 Parallel computer architecture. Top: Systolic arrays tile identical processing units for parallel processing. Here, instances of a multiply-and-add unit with input and output registers are chained to parallelize matrix multiplications. Bottom: Linking registers and processing units using the interleaving permutation as given by a perfect shuffle allows for parallelizing many useful computations, the most prominent example being the fast Fourier transform (FFT).

4.1 Parallel Computer Architecture

Already in the 1970s, the concepts of systolic arrays [KL79] and the perfect shuffle [Sto71] have been investigated in the context of parallel computer architecture.

Systolic arrays are based on simple processing units that are chained to form pipelines. As an example, the top of Fig. 4 shows a multiply-and-add-unit that computes $a \cdot x + b$. Both x and b are buffered by a register. Chaining multiple such compute units allows one to parallelize large parts of matrix multiplication. Obviously the latency of a systolic array pipeline is determined by the length of the chain of processing elements. The notion “systolic” stems from the analogy to the heart pumping in and out blood within a heartbeat, where in systolic arrays data is pumped in and out within a cycle. In fact, Google’s tensor processing units (TPU) are based on this architecture.

Perfect shuffle networks connect an array of registers to an array of processing units by the permutation resulting from perfectly interleaving two decks of cards one by one from each deck (see the bottom part of Fig. 4). The architecture has many famous applications, including the efficient implementation of the fast Fourier transform (FFT). The number of iterations is the latency, which amounts to the logarithm in base 2 of the number of registers, i.e. values to process.

Unrolling the iteration results in a structure reminiscent of the layer structure of artificial neural networks (see Fig. 1) and in fact has been tried to construct simple optical neural networks [RDZ00]. Yet, the connection pattern of the perfect shuffle appears to be too restrictive. In a series of articles [DBC17, DHBC18b, DHBC18a] more general permutations to connect layers have been explored. The permutations have their origins in interleaver design and interleaved codes. Visualizing the connection patterns in the unit square [DBC17, Figs. 4 and 5], where a point means a connection of the neuron at coordinate x to a neuron in the next layer at coordinate y in the subsequent layer, tends to make one think of sampling patterns as used in random number generation and quasi-Monte Carlo methods [Nie92].

4.2 Progressive Permutations

Many low discrepancy sequences are based on radical inversion. The principle is best explained by taking a look at the van der Corput sequence

$$\Phi_b : \mathbb{N}_0 \rightarrow \mathbb{Q} \cap [0, 1)$$

$$i = \sum_{l=0}^{\infty} a_l(i) b^l \mapsto \Phi_b(i) := \sum_{l=0}^{\infty} a_l(i) b^{-l-1}$$

in base $b \in \mathbb{N} \setminus \{1\}$ that maps the integers to the unit interval: Representing the integer i as digits $a_l(i)$ in base b and mirroring this representation at the decimal point yields a fraction between zero and one.

For contiguous blocks of indices $k \cdot b^m \leq i < (k+1) \cdot b^m - 1$ for any $k \in \mathbb{N}_0$, the radical inverses $\Phi_b(i)$ are equidistantly spaced. As a consequence of this perfect stratification, the integers $\lfloor b^m \Phi_b(i) \rfloor$ are a permutation of $\{0, \dots, b^m - 1\}$. Fixing b^m , k enumerates a sequence of permutations. As an example for $b = 2$, the first $2^4 = 16$ points yield the permutation

$$16 \cdot \Phi_2(i)|_{i=0}^{16} = (0, 8, 4, 12, 2, 10, 6, 14, 1, 9, 5, 13, 3, 11, 7, 15).$$

These properties are shared by the individual components of the s -dimensional sequence [Sob67], which may be the most popular low discrepancy sequence: Its first component is $x_i^{(0)} := \Phi_2(i)$, while the subsequent components

$$x_i^{(j)} = (2^{-1} \dots 2^{-m}) \cdot \underbrace{\left(C_j \cdot \begin{pmatrix} a_0(i) \\ \vdots \\ a_{m-1}(i) \end{pmatrix} \right)}_{\text{in } \mathbb{F}_2} \in \mathbb{Q} \cap [0, 1) \quad (5)$$

multiply a generator matrix C_j with the vector of digits before radical inversion. The generator matrices C_j are determined by the j -th primitive polynomial and for more details we refer to [Sob67, JK03, JK08, DP10].

The matrix vector multiplication takes place in the field \mathbb{F}_2 of two elements and very efficiently can be implemented using bit-wise parallel operations on unsigned integers. For each digit set in the integer i , the corresponding column of the generator vector just needs to be xor-ed with the so far accumulated value:

```
unsigned int x = 0;

for (unsigned int k = 0; i; i >>= 1, ++k)
    if (i & 1)
        x ^= C[k]; // parallel addition of column k of the matrix C
```

Experimenting with the Sobol' sequence [Sob67] is very practical, because an efficient implementation [JK03] along with the source code and optimized generator matrices has been provided at <https://web.maths.unsw.edu.au/~fkuo/sobol/>. Blocking groups of bits during radical inversion allows for an even faster generation of the Sobol' sequence, see [Wäc08, Listing 3.2].

The permutation properties described above are a consequence of each component of the Sobol' sequence being a $(0, 1)$ -sequence in base $b = 2$. As the Sobol' sequence produces Latin hypercube samples for each number of points being a power of 2, it can be used to create permutations in a progressive way. For more detail on (t, s) -sequences that in fact are sequences of (t, m, s) -nets, we refer to [Nie92, CH. 4].

4.3 Sampling Quasi-Random Paths

We will use the components of the Sobol' sequence instead of the pseudo-random number generator that sampled the path indices of the sparse networks in Sect. 3. As contiguous blocks of lengths of powers of 2 form permutations, we choose a power of 2 neurons per layer. This links the neural units

$$\left(a_{l, \lfloor n_l \cdot x_i^{(l)} \rfloor}, a_{l+1, \lfloor n_{l+1} \cdot x_i^{(l+1)} \rfloor} \right) \quad (6)$$

along the i -th path according to Eqn. 5. Similar to generating the paths by a pseudo-random number generator, the connectivity of the network does not need to be stored explicitly, because the components of the Sobol' sequence in Eqn. 5 can be computed on the fly. When the numbers of neurons in the input or output layer are not powers of two, one may choose to just fully connect these layers with their corresponding hidden layers.

The example in Fig. 5 demonstrates one advantage of encoding the network topology by a low discrepancy sequence. As the permutations are progressive, it is straightforward to add another power of 2 connections. Enumerating the network topology from sparse to fully connected becomes natural.

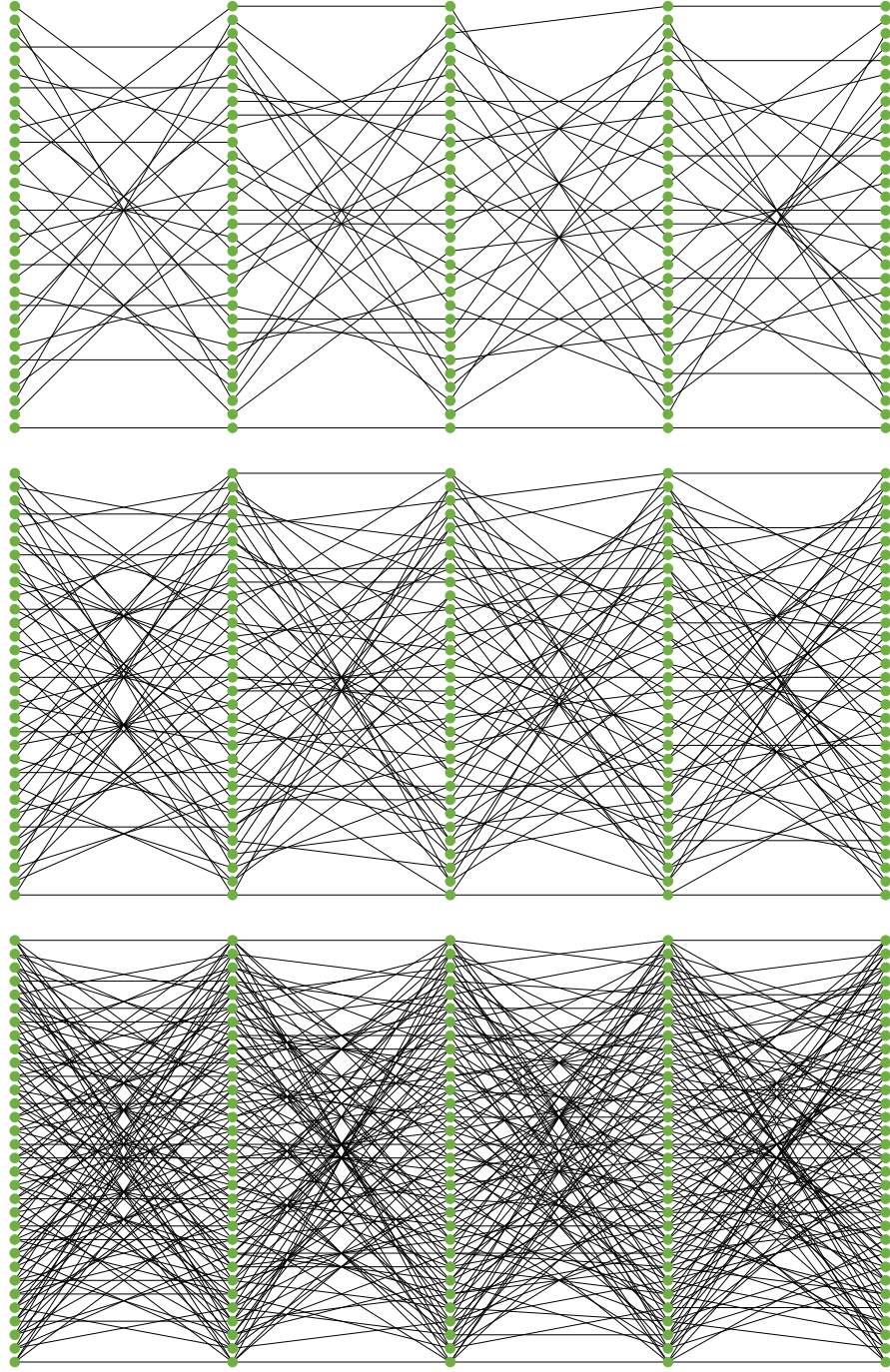


Fig. 5 Progressive enumeration of paths: For each 32 neural units in 5 layers, 32 (top), 64 (middle), and 128 (bottom) paths generated by the Sobol' sequence are shown. The number of paths per neural unit is 1, 2, or 4, respectively.

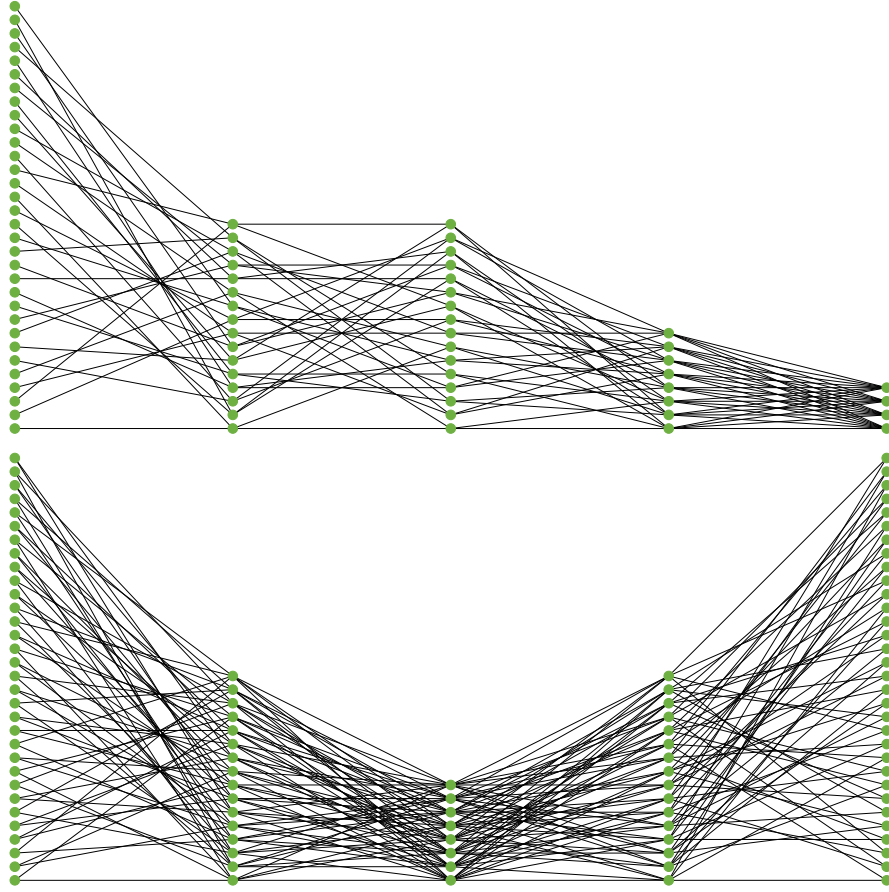


Fig. 6 Illustration of classic network architectures generated by the Sobol' sequence. Top: 32 inputs are encoded to 4 outputs. Such architectures are typically used for classification tasks. Bottom: 32 inputs are encoded to a latent space of 8 neural units and decoded back to 32 outputs. This is a common architecture of auto-encoders, whose typical task is filtering signals. Note that the number of neural units in each layer and the number of paths are powers of 2 and the fan-in and fan-out is constant across each layer.

Fig. 6 shows an example of a sparse classifier network generated by the Sobol' sequence. A high dimensional input vector on the left is condensed to a vector of classes on the right. Each layer has a power of 2 neurons and each neuron in a layer has the exact same constant number of connections. The next example is an autoencoder structure that is often used for filtering signals. Input and output layer are of the same dimension.

Creating a sparse network with non-negative weights like in Sec. 3.2 is as simple as selecting the first half of the paths to have non-negative weights and the second half to have non-positive weights. A second option is to dedicate one dimension of the Sobol' sequence to determine whether the weights of a path shall be non-negative

or non-positive just by checking whether the component is smaller than $\frac{1}{2}$ or not. More details on partitioning one low discrepancy sequence into many are found in [KG12]. If the number of paths is a power of 2, partitioning a network generated by the Sobol’ sequence into supporting and inhibiting network as described will result in a zero sum of weights per neuron if neurons in a layer have constant valence. This nicely complements the normalized initialization (see Sec. 3.1 and Sec. 3.3) and typically is not guaranteed when using a pseudo-random number generator to generate the paths.

Scrambling seed	Test accuracy	Test loss
not scrambled	78.51%	0.589
1174	81.64%	0.563
1741	79.30%	0.610
4117	80.08%	0.594
7141	77.73%	0.606

Table 1 Comparison of the test accuracy and loss with or without scrambling for sparse networks created by the Sobol’ sequence, skipping bad dimensions. The number of paths is 1024, hence the networks have 33754 weights. All networks are initialized with the same weights and training is deterministic, so the differences are only due to the connectivity patterns, some obviously being more accurate than others.

When the number of paths exceeds the product of the number of neurons in two successive layers, edges will be selected more than once. Even before reaching that bound and although the components of the Sobol’ sequence create progressive permutations, it may happen that multiple links as defined by Eqn. 6 coincide. While the algorithm in Fig. 3 automatically deals with multiple references¹, having multiple weights associated to one edge is redundant and may reduce the capacity of the network. The reason for this issue has been known for long from the domain of quasi-Monte Carlo methods and especially from the Sobol’ sequence, where low dimensional projections may expose very regular correlations between the dimensions. Ever since, low discrepancy sequences have been scrambled [Owe95] and optimized [JK03, Kel06]. Even a simple permutation of the order of the generator matrices C_j in Eqn. 5 or skipping dimensions can address the aforementioned issues. The effect of skipping dimensions that would lead to multiple references and scrambling is demonstrated in Table 1.

4.4 Hardware Considerations

Representing sparse networks by paths, the algorithm in Fig. 3 from Sec. 3 linearly streams the weights from memory. Such an access pattern perfectly matches the

¹ Note that emulating networks represented by paths using classic matrix-based machine learning frameworks results in multiple references to the same edge being coalesced in the corresponding matrix element.

parallel loading of contiguous blocks of weights in one cache line by the pre-fetcher as it is common for current processor hardware.

Similar to [DSCB17] and [DHBC18b, Fig. 4], the permutations generated by the Sobol' sequence guarantee streaming weights in contiguous blocks of size of a power of 2 free of memory bank conflicts. For the same reason, weights can be routed without collisions through a crossbar switch inside the processor. Both advantages cannot be guaranteed when creating paths by pseudo-random number generators.

Determining the permutations generated by Φ_2 in hardware amounts to bit reversal, which is straightforward to hardware. Implementing the permutations generated by Eqn. 5 in hardware requires to unroll the loop over the bit-parallel XOR operations (see the algorithm in Sec. 4.2). This results in a tiny circuit with a matrix of flip-flops to hold the generator matrix C_j . Replicating parts of the circuit for all numbers representable by the m least significant bits allows one to create 2^m values of the permutation in parallel.

For backpropagation, we can take advantage of the fact the the Sobol' sequence is invertible. Computing the inverse of Eqn. 5 just requires to determine C_j^{-1} . Propagating errors back through the network, the memory access pattern is not linear whenever the layer is changed. Still, memory is accessed in contiguous blocks within a layer.

5 Numerical Results

We perform numerical experiments to evaluate the accuracy of neural networks represented by paths generated by the Sobol' low discrepancy sequence. We take a look at classification tasks using classic multilayer perceptrons (MLP) as illustrated in Fig. 1, convolutional neural networks, the set of hyperparameters, and the initialization of sparse neural networks.

5.1 Training Sparse from Scratch

For the rather simple examples of recognizing digits or fashion items in tiny images (see Fig. 7), training a sparse-from-scratch artificial neural network and comparing it to its corresponding fully connected network reveals that only a tiny fraction of paths as compared to the number of connections within the fully connected layers is required to come very close to the test accuracy of the fully connected variant.

Comparing paths generated by pseudo-random numbers to paths generated by a low discrepancy sequence does not show any relevant discrepancy. However, as stated in Sec. 4.3, using the Sobol' low discrepancy sequence allows for routing without bank conflicts. This guarantee is a big advantage over pseudo-random number generated access patterns when considering a hardware implementation [DBC17, DHBC18b].

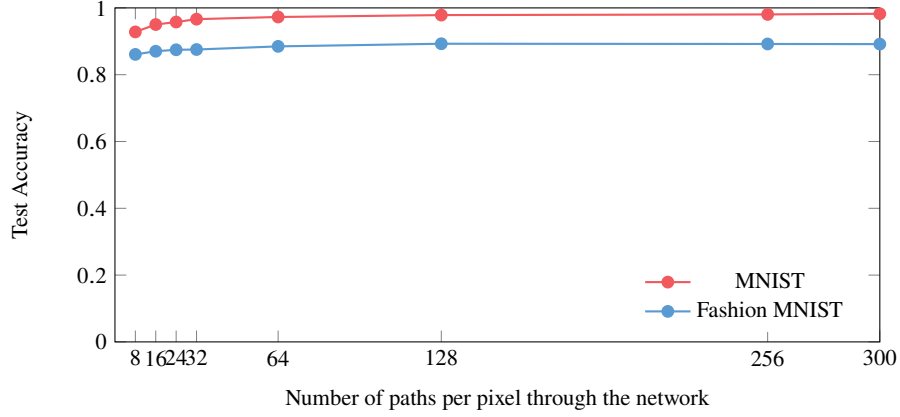


Fig. 7 Test accuracy of artificial neural networks represented by paths and trained sparse from scratch as compared to their fully connected counterparts. Only a tiny number of paths is required to reach the performance of the fully connected layers (300 paths per pixel) for the task of recognizing 10 classes of hand-written digits (MNIST) or fashion items (Fashion MNIST) in $784 = 28 \times 28$ pixel images. All networks have two hidden layers of 300 neurons each.

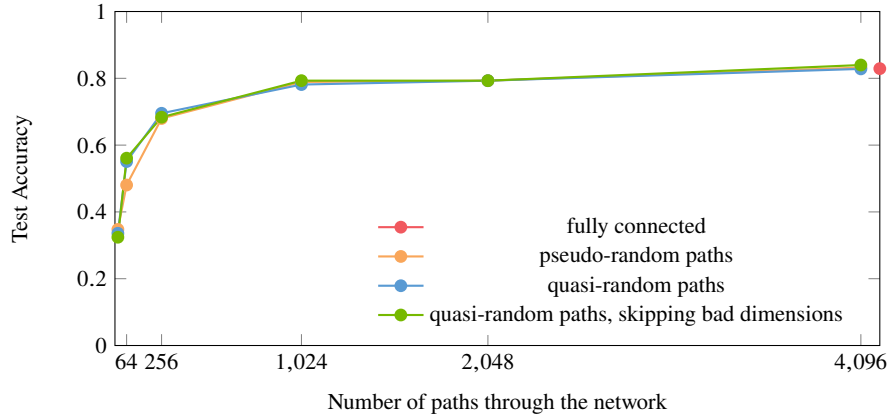


Fig. 8 Test accuracy of a convolutional neural network (CNN) represented by paths and trained sparse from scratch compared to their fully connected counterparts. The task is recognizing 10 classes of objects in 32×32 pixel images (CIFAR-10).

5.2 Random and Quasi-Random Paths in CNNs

Similar to the fully connected neural networks, convolutional neural networks (CNNs) represented by paths (see Sec. 2.2) can be trained sparse from scratch. For the numerical experiments, we use the CIFAR-10 image recognition data set. Our CNN has 5 convolutional layers with a number of channels 16, 32, 32, 64, 64, respectively, followed by one fully connected layer with a softmax activation func-

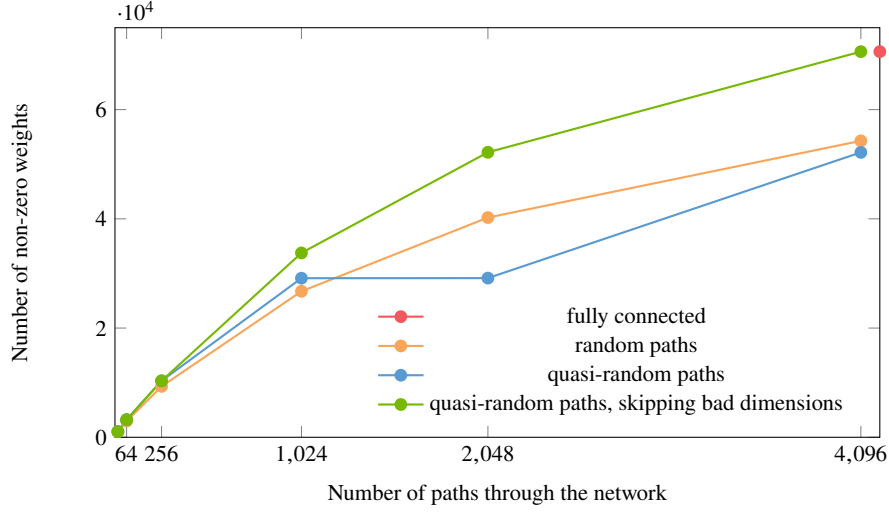


Fig. 9 The number of non-zero weights of a sparse convolutional neural network (CNN) represented by paths naturally is largest when avoiding coalescing edges. For the Sobol' sequence, this can be achieved by skipping dimensions of concern, while for random paths this simple remedy is not efficient. Note that for 1024 paths the accuracy already has reached a plateau (as shown in Fig. 8) and adding more paths cannot improve accuracy much, advocating sparse networks.

tion to produce 10 output features each identifying one of the dataset classes. Every convolutional layer is followed by a Batch Norm layer [IS15] and a ReLU activation function [GBB11]. Training is done for 182 epochs using stochastic gradient descent (SGD) with a momentum of 0.9. The learning rate starts at 0.1, and is decreased by factor 10 at epochs 91 and 136. We trained models with weight decay of 0.001 and 0.0001, and show the best obtained accuracy. We normalize the input images using the mean and standard deviation over the training set, and apply additional augmentation in the form of random horizontal flips as well as a 32×32 crop after padding the input image 4 pixels on every side.

Figure 8 shows the accuracy of sparse from scratch CNNs compared to a fully connected CNN, and Figure 9 shows the corresponding number of non-zero parameters. We observe a sharp increase in accuracy initially and then a slower convergence towards the accuracy of the fully connected network. Importantly, the graphs show that an accuracy close to the fully connected network can be reached with far less weights by uniformly sampling paths. The figure also shows that sampling paths randomly or quasi-randomly using the Sobol' sequence performs very similarly in terms of accuracy. However, as remarked in Section 5.1, there are large potential hardware advantages when using quasi-random methods.

5.3 Relation of Number of Paths, Layer Width, and Accuracy

The number of paths sampled gives fine control over the resulting sparsity, and hence over the computational complexity. We investigate how the accuracy and number of weights change when we scale the number of neurons per layer, i.e. the network width. In a fully connected network the number of weights increases quadratically with width. Selecting the convolutional neural network as in the previous section, we scale the width of every layer (except for the output layer) by a factor which we call the ‘width multiplier’. Keeping the number of sampled paths constant, the experiment shows an increase in accuracy up to a certain point, where accuracy starts degrading. This alludes to an optimal level of sparsity in the weights, see Figs. 10, 11 and 12.

Width multiplier	Number of paths	Sparsity	Test accuracy	Test loss
1.0	fully connected	0%	82.90%	0.523
1.25	4150	35.68%	83.59%	0.520
1.5	3050	55.23%	80.48%	0.495
2.0	2420	74.63%	83.20%	0.519
4.0	1950	93.59%	82.03%	0.544
8.0	1800	98.37%	77.34%	0.629

Table 2 Comparing fully connected narrow to wider, sparser networks created by random paths. The number of paths has been chosen such that all networks have around 70400 weights like the fully connected network with width multiplier 1.0. The network with lowest loss have width multiplier 1.5 and 2.0

It has been observed that wider but sparse networks have higher representational capacity than narrower dense networks [GRK17, CGRS19]. We verify this empirically in Table 2, where we compare several networks with a similar parameter count. We compare the fully connected network with width multipliers 1.0 to sparse networks with larger width multipliers, where we select the number of paths so that all networks have equivalent parameter count. We see that almost all sparse networks reach similar or higher accuracy than the fully connected network. If networks become too sparse, however, accuracy drops again.

Our observations are supported by learnings in neural network pruning and compression literature: neural networks are often compressible to 10%-20% of the fully connected counterpart [HLVDMW17]. Further compression results in significant loss in accuracy.

5.4 Initialization of Structurally Sparse Networks

Verifying the analysis from Sec. 3.1 and Sec. 3.2, we compare different initialization strategies and show the results in Table 3.

CNN	Initialization method	Test accuracy
Dense	Uniformly random	82.90%
	Constant, positive	10.02%
	Constant, alternating sign	10.00%
	Constant, random sign	82.43%
	Constant, random sign, 90% sparse	82.77%
Sparse	Uniformly random	78.91%
	Constant, positive	74.22%
	Constant, alternating sign	76.56%
	Constant, random sign	76.96%
	Constant, sign along path	78.13%
Sparse	Constant, alternating sign, signs fixed, train only magnitude	75.78%
	Constant sign along path, signs fixed, train only magnitude	68.76%

Table 3 Comparison of initializing weights uniformly random, constant positive, constant with half the initial values being negative, or constant but positive for odd neuron indices and negative otherwise (‘alternating’). The task is image classification with 10 classes (CIFAR-10). The sparse convolutional neural network (CNN) is created by tracing 1024 paths from the first layer. These sparse neural networks have 26.7K weights as compared to 70.4K for the dense net. ‘Signs non-trainable’ means that signs are kept fixed after initialization, while training only the weight magnitudes.

For the fully connected networks, setting all weights to the same value prevents learning completely as expected. Similarly using the same magnitude but setting the sign positive for weights with even index and negative otherwise (‘alternating’) makes the network too regular to learn. However, we see that simply choosing a random sign can result in very high accuracy, provided the constant w_{init} is chosen carefully as described in Section 3.1. We also find that initializing the weights sparse doesn’t hurt accuracy at all, and in fact seems to slightly improve it. With 90% sparsity, it can happen that a weight slice is completely zero at initialization. This is not a problem as long as there are nonzero values in the other filters belonging to that neuron.

For the sparse networks, we can make use of the paths for initialization, setting weights belonging to a path with an even index positive and negative otherwise. This can be done only for initialization or permanently in order to save one bit of storage per weight. The last 2 rows of Table 3 show what happens if the signs of the weights are fixed and we only train the weight magnitudes. The signs can be stored or generated dynamically as described in Sec. 3.2. Training only weight magnitudes, while initializing all weights with the same constant, the networks still reach accuracy within almost 3 % of the fully randomly initialized network.

Care needs to be taken when choosing to fix the sign for all weights along a path in a CNN. As not a single weight but a $w_f \times h_f$ filter slice is affected, enforcing the same sign for all these weights prevents the network from learning many types of features like edges. Still, such a sparse network using random paths is able to reach almost 70% accuracy. Note that this is not an issue for the common case of 1×1 convolutions, where $w_f = h_f = 1$.

The sparse networks are far more robust to the initialization and do not fail in any of the cases even with all weights in a layer set to the same positive constant. Using a deterministic low discrepancy sequence to enumerate the paths and to determine the signs of the weights allows for deterministic initialization and hence brings us one step closer to completely deterministic training.

6 Conclusion

Encoding the network topology by a deterministic low discrepancy sequence brings together quasi-Monte Carlo methods and artificial neural networks. The resulting artificial neural networks may be trained much more efficiently, because they are structurally sparse from scratch. In addition they allow for deterministic initialization. As shown for the example of the Sobol’ sequence, the resulting memory access and connection patterns are especially amenable to a hardware implementation, because they guarantee collision-free routing and constant valences across the neural units.

In future work, we will extend the investigations of quasi-Monte Carlo methods applied to other types of neural networks. Especially in the domain of speech recognition, preliminary experiments are very promising. Furthermore, we like to look at more low-discrepancy sequences and at growing neural networks during training by progressively sampling more paths as generated by the low discrepancy sequence.

Acknowledgements The first author is very thankful to Cédric Villani for a discussion on structure to be discovered in neural networks during the AI for Good Global Summit 2019 in Geneva. The authors like to thank Jeff Pool, Nikolaus Binder, and David Luebke for profound discussions and Noah Gamboa, who helped with early experiments on sparse artificial neural networks. This work has been partially funded by the Federal Ministry of Education and Research (BMBF, Germany) in the project Open Testbed Berlin - 5G and Beyond - OTB-5G+ (Förderkennzeichen 16KIS0980).

References

- CGRS19. Rewon Child, Scott Gray, Alec Radford, and Ilya Sutskever. Generating long sequences with sparse transformers. *arXiv preprint arXiv:1904.10509*, 2019.
- CSZ17. Soravit Changpinyo, Mark Sandler, and Andrey Zhmoginov. The power of sparsity in convolutional neural networks. *arXiv preprint arXiv:1702.06257*, 2017.
- DBC17. S. Dey, P. Beerei, and K. Chugg. Interleaver design for deep neural networks. In *51st Asilomar Conference on Signals, Systems, and Computers*, pages 1979–1983. IEEE, 2017.
- DHBC18a. S. Dey, K.-W. Huang, P. Beerel, and K. Chugg. Characterizing sparse connectivity patterns in neural networks. In *2018 Information Theory and Applications Workshop (ITA)*, pages 1–9. IEEE, 2018.
- DHBC18b. S. Dey, K.-W. Huang, P. Beerel, and K. Chugg. Pre-defined sparse neural networks with hardware acceleration. *CoRR*, abs/1812.01164, 2018.
- DP10. J. Dick and F. Pillichshammer. *Digital Nets and Sequences. Discrepancy Theory and Quasi-Monte Carlo Integration*. Cambridge University Press, 2010.

- dS16. Celso AR de Sousa. An overview on weight initialization methods for feedforward neural networks. In *2016 International Joint Conference on Neural Networks (IJCNN)*, pages 52–59. IEEE, 2016.
- DSCB17. Sourya Dey, Yinan Shao, Keith M. Chugg, and Peter A. Beerel. Accelerating training of deep neural networks via sparse edge processing. In Alessandra Lintas, Stefano Rovetta, Paul F.M.J. Verschure, and Alessandro E.P. Villa, editors, *Artificial Neural Networks and Machine Learning – ICANN 2017*, pages 273–280, Cham, 2017. Springer International Publishing.
- DZ19. Tim Dettmers and Luke Zettlemoyer. Sparse networks from scratch: Faster training without losing performance. *CoRR*, abs/1907.04840, 2019.
- FC19. Jonathan Frankle and Michael Carbin. The lottery ticket hypothesis: Finding sparse, trainable neural networks. In *ICLR*. OpenReview.net, 2019.
- FPPP85. Nabil H. Farhat, Demetri Psaltis, Aluizio Prata, and Eung Paek. Optical implementation of the Hopfield model. *Appl. Opt.*, 24(10):1469–1475, May 1985.
- GBB11. Xavier Glorot, Antoine Bordes, and Yoshua Bengio. Deep sparse rectifier neural networks. In *Proceedings of the fourteenth International Conference on Artificial Intelligence and Statistics*, pages 315–323. JMLR Workshop and Conference Proceedings, 2011.
- GRK17. Scott Gray, Alec Radford, and Diederik P Kingma. GPU kernels for block-sparse weights. *arXiv preprint arXiv:1711.09224*, 3, 2017.
- HBO⁺19. E. Heitz, L. Belcour, V. Ostromoukhov, D. Coeurjolly, and J.-C. Iehl. A low-discrepancy sampler that distributes Monte Carlo errors as a blue noise in screen space. In *SIGGRAPH’19 Talks*, Los Angeles, United States, July 2019. ACM.
- HLVDMW17. Gao Huang, Zhuang Liu, Laurens Van Der Maaten, and Kilian Q. Weinberger. Densely connected convolutional networks. In *Proceedings of the IEEE conference on computer vision and pattern recognition*, pages 4700–4708, 2017.
- HZRS15. Kaiming He, Xiangyu Zhang, Shaoqing Ren, and Jian Sun. Delving deep into rectifiers: Surpassing human-level performance on imagenet classification. In *Proceedings of the IEEE international conference on computer vision*, pages 1026–1034, 2015.
- IS15. Sergey Ioffe and Christian Szegedy. Batch normalization: Accelerating deep network training by reducing internal covariate shift. In *International Conference on Machine Learning*, pages 448–456. PMLR, 2015.
- JK03. S. Joe and F. Kuo. Remark on algorithm 659: Implementing Sobol’ quasirandom sequence generator. *ACM Trans. Math. Softw.*, 29(1):49–57, 2003.
- JK08. S. Joe and F. Kuo. Notes on generating Sobol’ sequences. Technical report, School of Mathematics and Statistics, University of New South Wales, 2008.
- JPR⁺20. Siddhant Jayakumar, Razvan Pascanu, Jack Rae, Simon Osindero, and Erich Elsen. Top-KAST: Top-k always sparse training. *Advances in Neural Information Processing Systems*, 33, 2020.
- KBG⁺20. S. Krizan, S. Beliaev, B. Ginsburg, J. Huang, O. Kuchaiev, V. Lavrukhin, R. Leary, J. Li, and Y. Zhang. Quartznet: Deep automatic speech recognition with 1d time-channel separable convolutions. In *ICASSP 2020 - 2020 IEEE International Conference on Acoustics, Speech and Signal Processing (ICASSP)*, pages 6124–6128, 2020.
- Kel06. A. Keller. Myths of computer graphics. In H. Niederreiter, editor, *Monte Carlo and Quasi-Monte Carlo Methods 2004*, pages 217–243. Springer, 2006.
- Kel13. A. Keller. Quasi-Monte Carlo image synthesis in a nutshell. In J. Dick, F. Kuo, G. Peters, and I. Sloan, editors, *Monte Carlo and Quasi-Monte Carlo Methods 2012*, pages 203–238. Springer, 2013.
- KG12. A. Keller and L. Grünschloß. Parallel quasi-Monte Carlo integration by partitioning low discrepancy sequences. In L. Plaskota and H. Woźniakowski, editors, *Monte Carlo and Quasi-Monte Carlo Methods 2010*, pages 487–498. Springer, 2012.
- KL79. H. Kung and C. Leiserson. Systolic arrays (for VLSI). *SIAM Sparse Matrix Proc.* 1978, pages 256–282, 1979.

- KNP⁺20. Souvik Kundu, Mahdi Nazemi, Massoud Pedram, Keith M. Chugg, and Peter A. Beerel. Pre-defined sparsity for low-complexity convolutional neural networks, 2020.
- KPA⁺19. Souvik Kundu, Saurav Prakash, Haleh Akrami, Peter A. Beerel, and Keith M. Chugg. pSConv: A pre-defined sparse kernel based convolution for deep CNNs. In *2019 57th Annual Allerton Conference on Communication, Control, and Computing (Allerton)*, pages 100–107, 2019.
- LBBH98. Y. Lecun, L. Bottou, Y. Bengio, and P. Haffner. Gradient-based learning applied to document recognition. *Proceedings of the IEEE*, 86(11):2278–2324, 1998.
- MkK19. G. Mordido, M. Van keirsbilck, and A. Keller. Instant quantization of neural networks using Monte Carlo methods. *NeurIPS 2019 5th Workshop on Energy Efficient Machine Learning and Cognitive Computing (NeurIPS 2019 EMC²)*, 2019.
- MkK20. G. Mordido, M. Van keirsbilck, and A. Keller. Monte Carlo gradient quantization. *CVPR 2020 Joint Workshop on Efficient Deep Learning in Computer Vision (CVPR 2020 EDLCV)*, 2020.
- MMT⁺19. Pavlo Molchanov, Arun Mallya, Stephen Tyree, Iuri Frosio, and Jan Kautz. Importance estimation for neural network pruning. In *Proceedings of the IEEE/CVF Conference on Computer Vision and Pattern Recognition*, pages 11264–11272, 2019.
- Nie92. H. Niederreiter. *Random Number Generation and Quasi-Monte Carlo Methods*. SIAM, Philadelphia, 1992.
- Owe95. A. Owen. Randomly permuted (t, m, s) -nets and (t, s) -sequences. In H. Niederreiter and P. Shiue, editors, *Monte Carlo and Quasi-Monte Carlo Methods in Scientific Computing*, volume 106 of *Lecture Notes in Statistics*, pages 299–315. Springer, 1995.
- RDZ00. X. Rui, H. Daquan, and L. Zhineng. A perfect shuffle type of interpattern association optical neural network model. *Guangzi Xuebao/Acta Photonica Sinica*, 29(1), 01 2000.
- RHW88. D. Rumelhart, G. Hinton, and R. Williams. Learning representations by back-propagating errors. In J. Anderson and E. Rosenfeld, editors, *Neurocomputing: Foundations of Research*, pages 696–699. MIT Press, Cambridge, MA, USA, 1988.
- Sob67. I. Sobol’. On the Distribution of points in a cube and the approximate evaluation of integrals. *Zh. vychisl. Mat. mat. Fiz.*, 7(4):784–802, 1967. USSR Comput. Math. Math. Phys., pp. 86–112.
- Sto71. H. Stone. Parallel processing with the perfect shuffle. *IEEE Trans. Comput.*, 20(2):153–161, February 1971.
- Wäc08. C. Wächter. *Quasi-Monte Carlo Light Transport Simulation by Efficient Ray Tracing*. PhD thesis, Universität Ulm, 2008.
- ZHMD16. C. Zhu, S. Han, H. Mao, and W. Dally. Trained ternary quantization. *CoRR*, abs/1612.01064, 2016.
- ZLLY19. Hattie Zhou, Janice Lan, Rosanne Liu, and Jason Yosinski. Deconstructing lottery tickets: Zeros, signs, and the supermask. In *NeurIPS 2019*, 2019. arXiv:1905.01067.

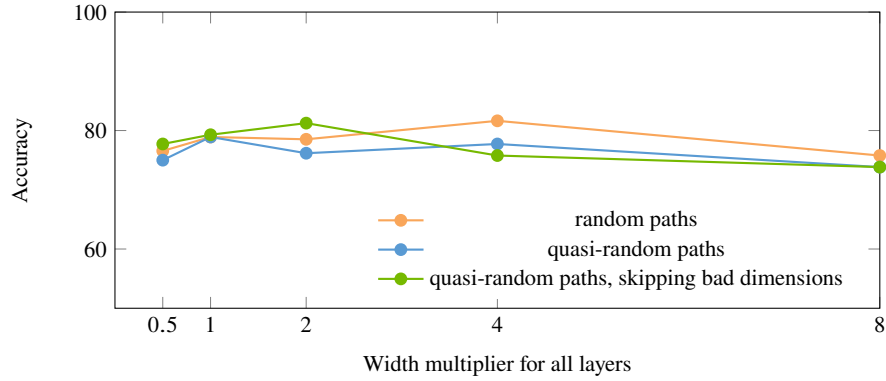


Fig. 10 Accuracy of sparse convolutional neural networks represented by paths, scaling the width of the network with the number of paths fixed to 1024. The highest accuracies are reached for widths 1-4, where networks are sparse but not extremely sparse (see Figure 12)

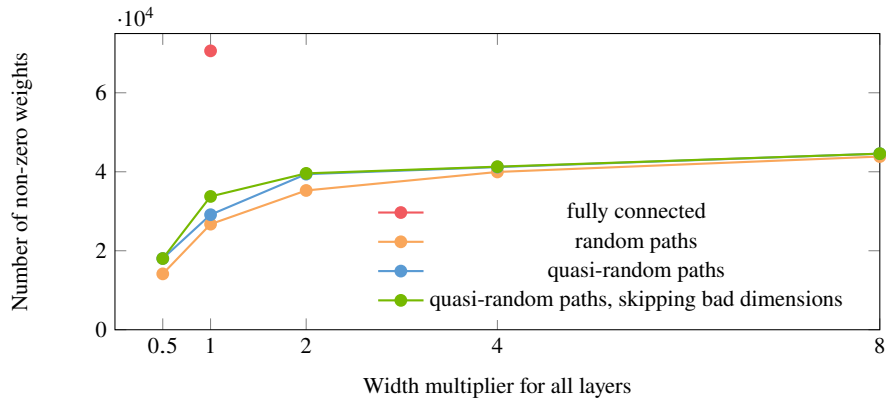


Fig. 11 Number of non-zero weights of sparse convolutional neural networks represented by paths, scaling the width of the network with the number of paths fixed to 1024. For very narrow networks, they are close to full connectivity and the number of weights only grows if the network width is increased. For wide networks, the number is limited by the number of paths.

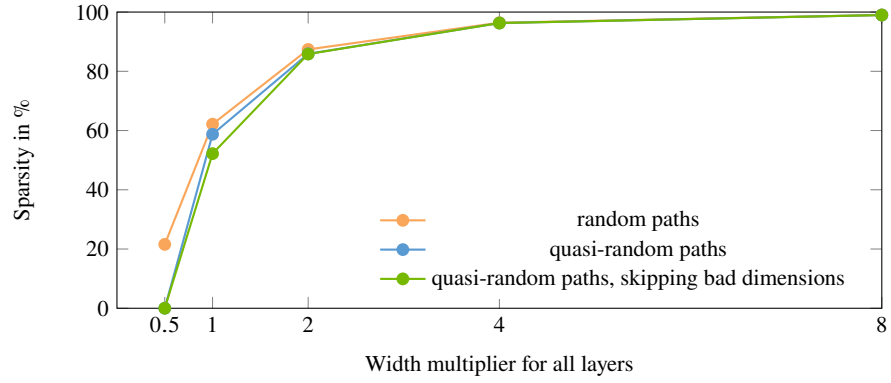


Fig. 12 Sparsity of sparse convolutional neural networks represented by paths, scaling the width of the network while the number of paths remains fixed to 1024. Since the number of paths directly controls the number of weights, and the number total possible connections grows quadratically in the network width, wider networks get sparse very quickly.